JOURNAL OF MATERIALS SCIENCE 9 (1974) 1917–1925

The growth morphology of the Ni-rich Ni-Ta-Cr-Mn system

G. PIATTI, J. DEJACE, C. FOSSATI, R. MATERA
Euratom Joint Research Center, Materials Division, Ispra, Italy

The solidification of an Ni–Ta–Cr–Mn alloy has been investigated for a range of cooling rates and the cellular-to-dendrite transition characterized. The growth directions of the primary and secondary dendrite branches are parallel to ⟨100⟩. Microsegregation produces a white core in the dendrite interior in some growth conditions.

1. Introduction

A previous paper [1] described some experimental observations of dendrite crystals grown in complex Ni-base alloys (mean composition Ni 57, Ta 21, Cr 15, and Mn 7 wt. %) carried out by the authors. The topography of the dendrites was studied by electron scanning microscopy and the structure by X-rays. It has been shown that the dendrites in the complex system investigated grow as single-phase Ni-rich solution with Ta, Cr and Mn, and are transformed into duplex crystals by Widmanstätten precipitation of a second phase (Ni_3Ta–β) owing to large variation with temperature of solubility of Ta in Ni.

The system investigated was based on the eutectic Ni–Ni_3Ta which reveals, under certain experimental conditions of unidirectional solidification, an oriented lamellar type structure with an Ni(Ta) solid solution as matrix and Ni_3Ta as second phase [2, 3]. The addition to this system of a third (Cr) and a fourth (Mn) element leads to a breakdown of the regular planar solidification front into cells or dendrites [1] depending upon growth conditions, as might be expected on the basis of observations of different researchers in the fields of unidirectional solidification of binary eutectics containing ternary additions [4-6].

In the present work, the cell-to-dendrite transition and the dendrite evolution are examined from a morphological point of view in the Ni–Ta–Cr–Mn system within a given composition range as a function of the unidirectional solidification rate using different experimental techniques. A decanting technique was also employed in order to obtain free dendrites, always in the investigated Ni–Ta–Cr–Mn system, with the aim of obtaining additional information on the dendrite morphology and particularly on dendrite tips and branches grown in the liquid. Different authors [7-10] obtained dendrite structures by liquid decanting during various conditions of steady-state growth in order to observe the topography of the dendrites and to study the growth mechanism.

The system Ni–Ta–Cr–Mn is also investigated from the point of view of crystallographic structure and dendrite microsegregation phenomena. This latter causes the presence of an unusual white core in the interior of the dendrite substructure. It has been shown [11] that in dendritic structures there is very strong segregation.

2. Experimental

The samples showing dendrite morphology were prepared for experimental observation as follows:

(a) Elaboration by arc-melting of small ingots (mean composition Ni 57, Ta 21, Cr 15, and Mn 7 wt. %) starting from pure elements (Ni 99.8, Ta 99.8, Cr 99.9 and Mn 99.9);

(b) Remelting of the ingots in an induction furnace in alumina crucibles (argon atmosphere) with the production of 15 bars, 8 mm in diameter and 150 mm in length;

(c) Unidirectional solidification of the previously prepared bar on an apparatus described elsewhere [12] and suitably modified in order to overcome the difficulties of compatibility problems between the Ni–Ta–Cr–Mn alloy and the container. Alumina cylindrical crucibles (i.d. 10 mm) were employed in an argon atmosphere,

TABLE I Experimental details

Alloy	Solidification rate R (cm/h)	Substructure morphology
1	0.41	Regular cells
2	0.85	Flanged cells or cellular dendrites
3	1.7	Cellular dendrites exhibiting the start of periodical lateral branching
4	4.9	Dendrites like rod branched type
5	9.3	Dendrites like rod branched type
6	9.5	Dendrites like rod branched type with white core
7	9.6	Dendrites like rod branched type with white core
8	10.1	Dendrites like rod branched type with white core
9	10.1	Dendrites like rod branched type with white core
10	10.1	Dendrites like rod branched type with white core
11	10.1	Dendrites like rod branched type with white core
12	13.8	Dendrites like rod branched type with white core
13	26	Dendrites like rod branched type with white core
14	27.6	Dendrites like rod branched type with white core
15	42	Dendrites (no core)
Arc-cast structure	—	Irregular dendrite structure
Induction melted structure	—	Irregular dendrite structure
Decanting technique	—	Free dendrites

heating with a platinum resistor and cooling with water. In order to investigate the dendrite morphology under steady-state growth conditions, all bars were solidified at different rates (R) which are listed in Table I. The thermal gradient (G) was of the order of 145 to 150°C cm^{-1}. It was measured by immersion in the liquid metal, under steady-state conditions, of a thermocouple protected from corrosion by an alumina coating;

(d) Final preparation of samples for the different experimental observations. Metallographic specimens were taken near the centre of each bar (transverse and longitudinal sections) and prepared by polishing with diamond paste and two-step etching with the following solutions: (A) 5% H_2SO_4–95% H_2O (1.5 V, 15 sec) and (B) 33.3% HNO_3 33.3% HF–33.3% glycerol. Some specimens were also prepared for observation by scanning electron microscope (JEOL-JFM/U3) by a deep chemical etching with solution (B). Thin foils were obtained from one of the alloys by electrochemical thinning for electron microscope examination in a Philips EM 300 microscope (transmission and electron diffraction). Some replicas were also prepared for observation under electron microscope. Moreover, in some cases, the dendrite structure was analysed using an electron probe microanalyser (Cameca). X-ray diffraction techniques were also employed. In order to obtain a better evaluation of dendrite substructure, some specimens were prepared for Vickers microindentation (Leitz microhardness tester, load 100 g; Reichert apparatus, load 2 and 5 g);

(e) Free dendrites of the same composition as the unidirectionally solidified alloys, obtained by a natural decanting technique, were examined by scanning electron microscopy and X-ray diffraction.

3. Results

3.1. Undirectional structure

The examination of the master ingots (arc-cast and induction-melted) revealed an irregular dendrite structure, some dendrite branches being very long and others very short. On the other hand, no dendrites were observed at the slowest solidification rate employed (R = 0.41 cm h^{-1}). In this case, a cellular substructure was present, the cells showing regular size and geometry.

At the next solidification rate (R = 0.85 cm h^{-1}) a cellular dendrite substructure appears. This morphology is characterized by cellular dendrites in straight columns with continuous flanges. Similar structures were observed in Pb–Sb systems by other authors and have been named "flanged-cells" [13]. At R = 1.7 cm h^{-1}, a periodic lateral branching appeared and, at higher solidification rates, the substructure turned into a dendrite type with a regular array of dendrite rows (Fig. 1). The cross-section of a

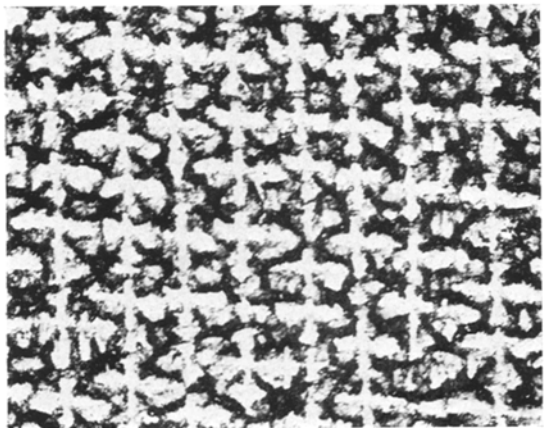

Figure 1 A transverse section of a solidified bar of alloy 4 (R = 4.9 cm h^{-1}) showing regular array of cellular dendrites of the cruciform type. Etching A/B. (× 20).

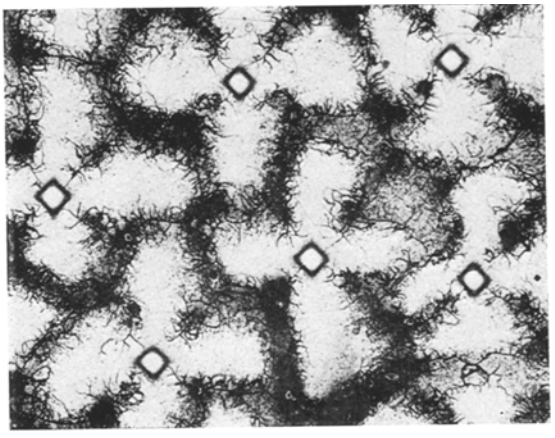

Figure 2 Transverse sections of a solidified bar of alloy 6 (R = 9.5 cm h^{-1}) at different magnification showing a white core in every dendrite element. Etching A/B. (× 100).

single dendrite showed a cruciform type similar to examples given in the literature for other metals or alloys with cubic crystal structure [14-20]. The morphology was not plate-like but more resembles the rod-branched type. At R = 9.5 cm h^{-1} the single dendrite element, without changing its morphology, exhibited a white core (Fig. 2), the size of this core increasing from the bottom to the top of the bars. This

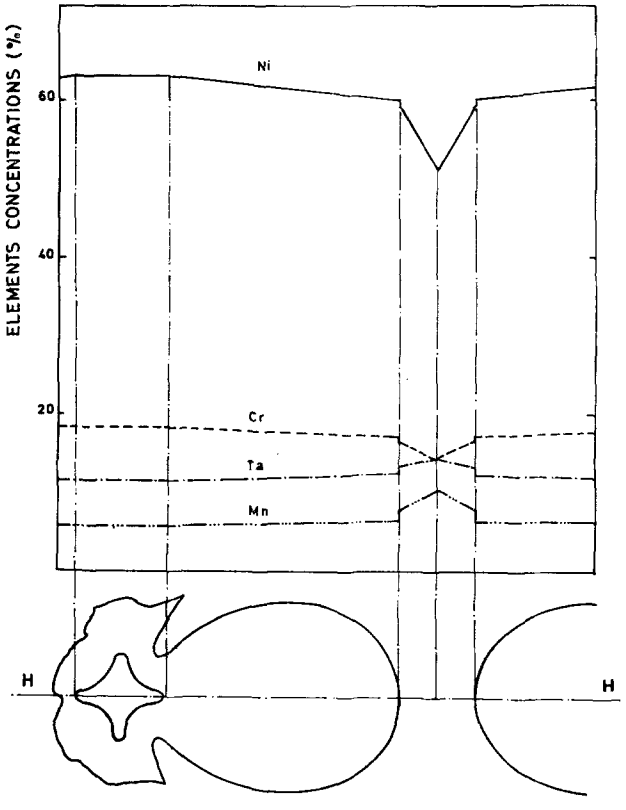

Figure 3 Wt. % concentrations of single elements (Ni, Ta, Cr, Mn) along the line H-H in a transverse section to the growth direction (alloy 6).

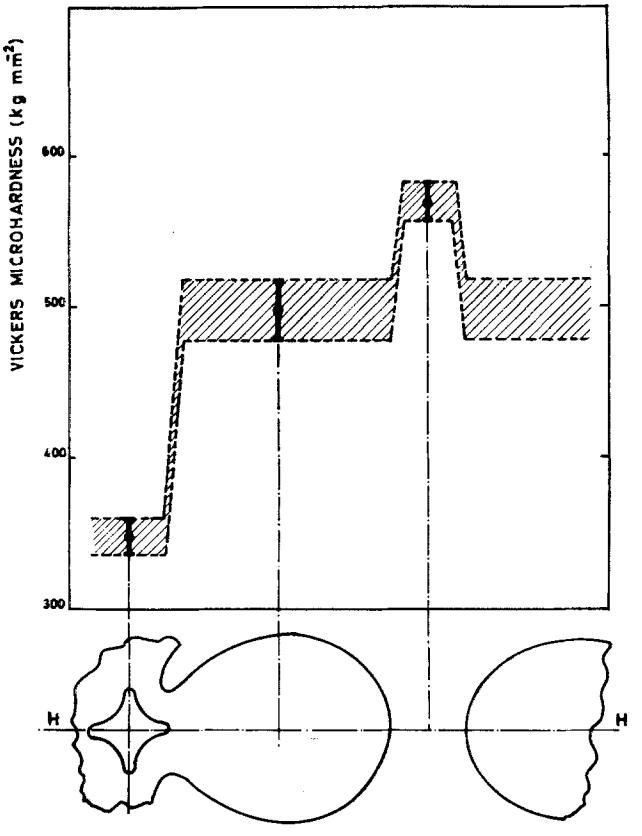

Figure 4 Microhardness (Vickers) values on the H-H line on a cross-section to the growth direction. The mean values are based on ten readings (alloys 12 and 14).

structure was present also at higher solidification rates and disappeared only at the highest value investigated (R = 42 cm h^{-1}).

The electroprobe microanalyses are shown in Fig. 3. It is quite clear that Ta and Mn are concentrated in the interdendritic spacing where the concentration of Ni and Cr decreases and a relatively strong segregation is shown. A decrease in total Ta concentration in comparison with the initial value has also been observed. A discontinuity along the axis of the dendrite branches was shown also by microhardness (Vickers) indentations presented in Fig. 4. Not only was there an increase in hardness values in the transition zone from dendritic to interdendritic, but also from white core to dendritic arm. The Reichert microhardness indentations performed on different specimens along the axis of dendritic branches also confirm this trend.

From a structural point of view, X-ray diffraction analysis by the Guinier technique on powder obtained by mechanical filing confirms the lines of Ni solid solution and the principal lines of the $Ni_3Ta\beta$ (tetragonal) intermetallic compound as expected. The structure identification is clearer from electron transmission microscopy and electron diffraction (Figs. 5 and 6). A two-phase structure was evident: an Ni solution matrix with oriented precipitates of $Ni_3Ta\beta$. An intermetallic precipitation was also visible with optical microscopy in the interdendritic region of all samples. An example is shown in Fig. 7.

3.2. Decanting technique morphology

Decanted interfaces (Fig. 8) reveal clearly how dendrite branches and tips propagate in the liquid. The solidification rate is in this case unknown, but was certainly less than the value adopted in unidirectional solidification experiments. The free dendrites showed the classical shape of the rod-like dendritic type with periodical lateral secondary branching and, in some cases, tertiary and even higher-order arms. The

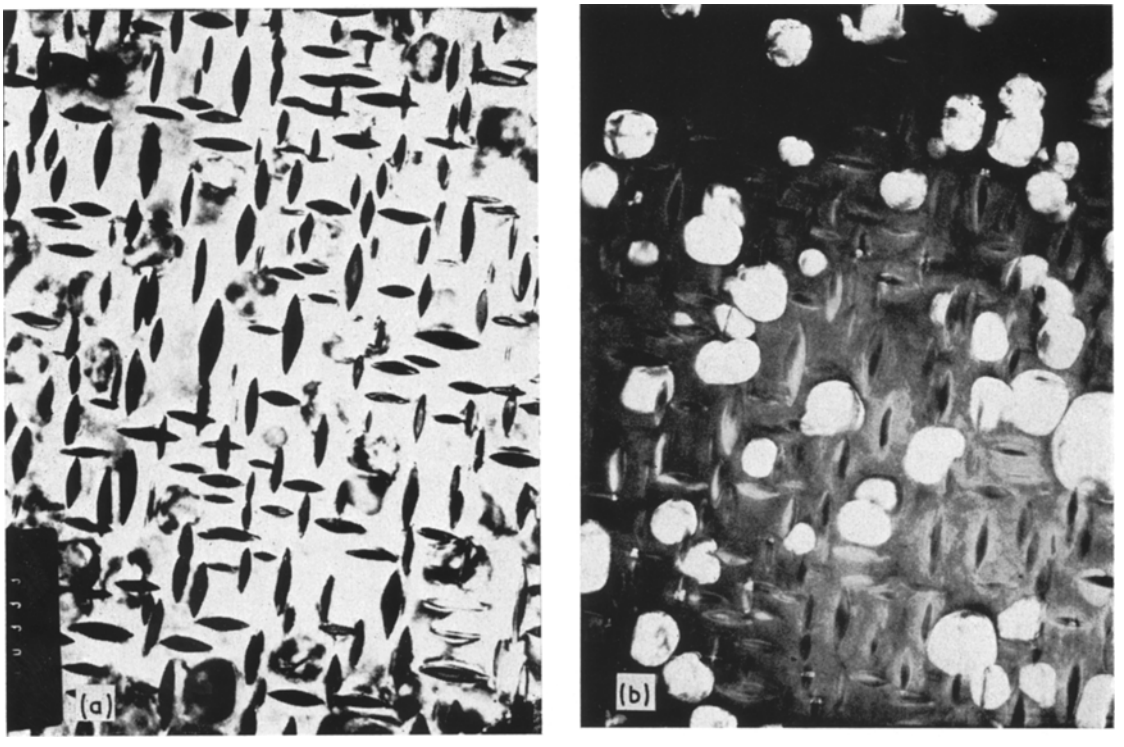

Figure 5 Transmission electron micrographs of a thin foil of alloy 12. (a) Bright field (× 46 000), (b) dark field (× 46 000).

Figure 6 Diffraction pattern of selected area of Fig. 5 showing matrix and three precipitate reflections.

arms were generally more developed than in the case of the unidirectionally solidified bar. Another observation was that the dendrites were aligned in a periodic array.

X-ray technique results published previously [1] have shown that the structure of free

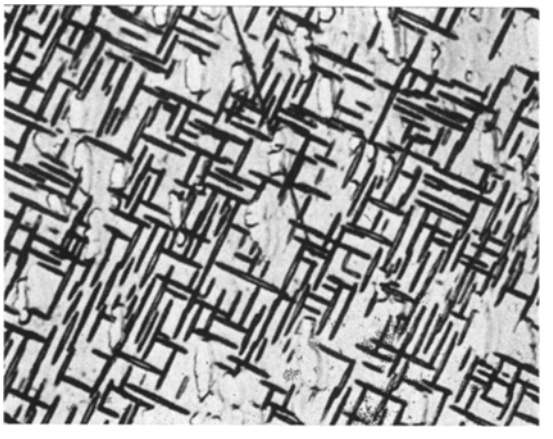

Figure 7 Widmanstätten precipitation in the interdendritic region on alloy 1. Etching A/B. (× 1000).

Figure 8 Free dendrites obtained by decanting technique (scanning electron microscope image). No etching. (× 100).

dendrites is duplex-crystal type, that is Ni solution matrix (a = 3.62 Å) with three families of precipitates with the three possible cubic orientations:

(001) prec. ∥ {100} matrix
[010] prec. ∥ ⟨100⟩ matrix .

The second phase precipitates were identified as tetragonal with lattice parameters a = 3.62 Å, c = 7.46 Å, c/a = 2.06, which correspond to an $Ni_3Ta\beta$ structure [21]. This duplex crystal structure corresponds to the results of electron diffraction mentioned in Section 3.1.

4. Discussion

4.1. Substructure morphology

From a general point of view the cellular-to-dendrite transition is gradual and continuous as has been illustrated by different authors [13, 22, 23]. However, for convenience, four discrete stages can be assumed from experimental observations (Section 3.1). These are:

(1) regular cells;

(2) cellular dendrites or flanged cells;

(3) cellular dendrites exhibiting the start of periodic lateral branching;

(4) rod-branched type dendrites with primary [100], secondary [010], and tertiary [001] arms. This morphology also corresponds to that of free dendrites obtained by decanting techniques.

Similar cellular-to-dendrite evolution was found by other authors. The first three stages correspond to a schematic illustration of the changing shape of the growth structure as the solidification rate is increased, proposed by Morris and Winegard ([13], Fig. 5) for the Pb–Sb system. The transition from stage 3 to stage 4 has also been illustrated schematically ([24], Fig. 5) by Kurtz and Lux, as a function not only of an increase in solidification rate but also of a decrease in thermal gradient. On the other hand, Chalmers has discussed [25] comprehensively the cellular dendrite–free dendrite evolution based on the constitutional supercooling criterion (C.S.) with a variation in thermal gradient from positive to zero or negative values. According to other authors, the transition from cellular to dendrite substructure seems to be governed by the ratio $G/R^{\frac{1}{2}}$ [22, 26, 27] and G/R [28], but the application of a simple C.S. criterion for the transition mentioned has since been questioned [29].

As the quantitative values of the thermal gradient were not known with any certainty, it was impossible to verify the previously cited models based on constitutional supercooling. Moreover, the presence of a large percentage of different solutes makes it very difficult to assume that the solution is dilute and that there is no interaction between solutes, which is an essential condition for the application of the well-known solidification theories.

4.2. Microsegregation

Microsegregation effects on unidirectionally solidified structures are clearly visible not only from dendrite substructure but more quantitatively from microprobe analysis and microhardness tests (Figs. 3 and 4). The trend of increase of the solute elements Ta and Mn on going out radially from the dendrite core were expected. On the other hand Cr behaviour has been an exception difficult to explain. However, the singular effect of the segregation is the white core present in the solidified bar from R = 9.5 cm h^{-1} to R = 27.6 cm h^{-1}. An explanation of this can be given starting from the hypothesis that compositions investigated in the Ni–Ta–Cr–Mn system correspond to equilibrium conditions at temperature ∼ 1200° C (melting point of the Ni–Ta–Cr–Mn alloy investigated ∼ 1280° C), to a single phase (complete Ni solid solution), but at room temperature there is a two-phase structure (Ni solid solution plus a second phase composed of an intermetallic $Ni_3Ta\beta$ type compound). If we consider now the segregation phenomena due to rapid cooling of the solid solution from the liquid state, an

inhomogeneous structure is produced and non-equilibrium solidification is obtained, as shown for the Al–Cu system [30]. The mechanism is shown schematically in Fig. 9. A quaternary system is appropriate to the present case, so that for the plotting of the alloy composition the use of a tetrahedron is necessary (Fig. 9a). As the Ta concentration changes, the alloy composition follows the A-B line. The temperature concentration diagram of this line is reported schematically in Fig. 9b. Now if we suppose that the non-equilibrium solvus line $C'_s - C''_s$ is to the left of the equilibrium solvus line, not only is the dendrite substructure two phase but there are two zones: the inner zone (white core) as a single-phase Ni solution, and the more external

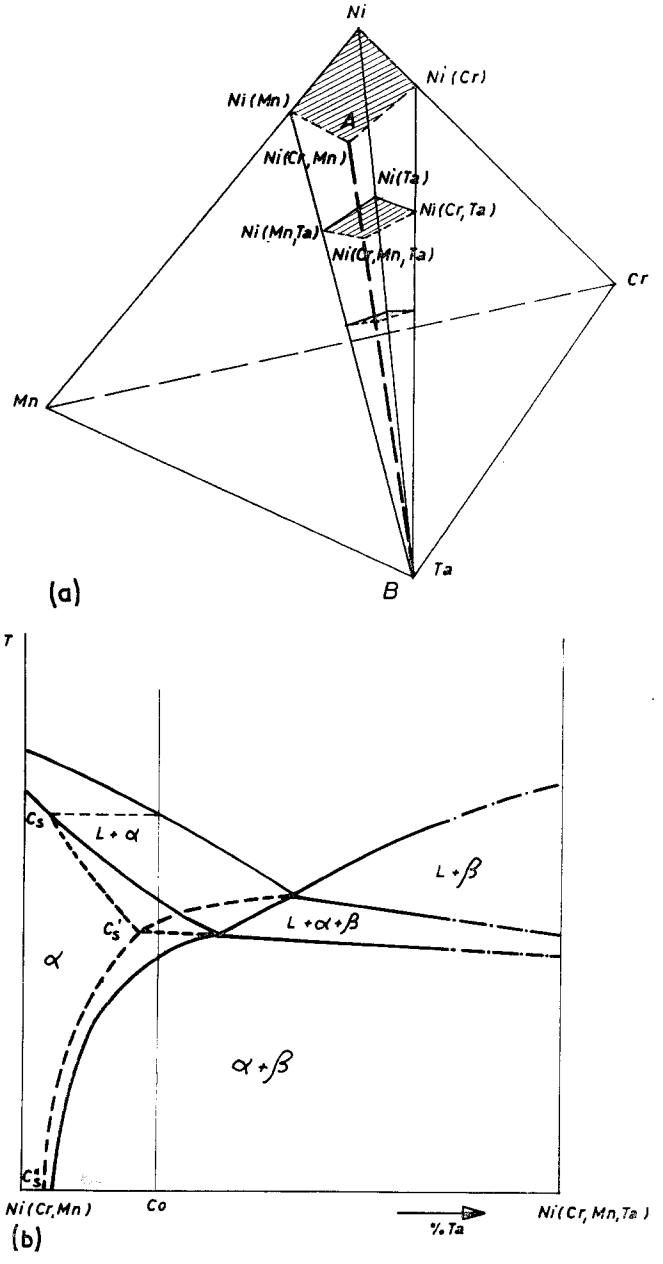

Figure 9 Qualitative explanation of the non-equilibrium solidification mechanism. (a) Plotting of alloy composition in quaternary system; (b) two dimensional temperature-concentration diagram for the A-B line on (a).

grey zone as a two-phase structure of matrix plus intermetallic compound (Fig. 2). This justification is not sufficient to explain why the white core is not present over the whole rate range investigated. It is necessary to suppose that a decrease in Ta solute concentration, as shown by the microprobe analysis is due to oxidation phenomena which are dependent upon, and not linear with, time. The decrease in Ta is particularly noticeable at a low solidification rate as proved by the electron probe analysis; therefore, it is evident that solidification rates play an important role in the behaviour of the white core. For high values of R the effective solidification curve is quite different from that of the equilibrium but the Ta concentration remains too high, thus causing segregation in the whole dendrite. On the contrary, for low values of R, even if the Ta concentration decreases to a noticeable extent, the alloy follows a $C_s - C''_s$ line which practically coincides with the equilibrium one causing once again a complete segregation. For intermediate values of R the Ta concentration and pseudo-equilibrium curves allow the centres of the dendrites to have a low solute concentration, stable in the α phase even at room temperature. Replica stages of the white core observed through an electron microscope do not show two phases even at high magnification. Microhardness results are also consistent with the single-phase nature of the white core (low values of hardness due to solution hardening) and the two-phase nature of the rest (high values of hardness due to precipitation hardening).

4.3. Crystallographic structure

If the previous results [1] on free dendrites are taken into account, the experimental investigation (X-ray diffraction and electron diffraction), together with the previous considerations, confirms that there is a two-phase structure in the dendritic substructure: an Ni matrix solid solution plus a second phase of the intermetallic compound βNi_3Ta type as fine Widmanstätten precipitates. The interdendritic material also contains two phases, always an Ni matrix solid solution with a second phase coarse, Widmanstätten structure of intermetallic type. This Widmanstätten structure is probably also composed of βNi_3Ta type, since no other phase was identified by X-rays. On the contrary, when the decanting technique is used to prepare free dendrites, the residual interdendritic liquid solidifies into a lamellar structure (Fig. 10); these lamellae were analysed by the single crystal X-ray diffraction technique: they have an orthorhombic lattice which corresponds to the $Ni_3Ta\alpha$ type of structure [31]. On the other hand, under equilibrium conditions at high temperature, there is a single-phase Ni solid solution, but at room temperature the alloy adopts a two-phase structure, with the second phase always consisting of Widmanstätten type. This is due to the great variation in solubility of Ta in Ni with temperature [32].

5. Conclusions

The analysis of different experimental results in an Ni corner Ni–Ta–Cr–Mn system, both unidirectionally solidified at different solidification rates (R = 0.41 to 42 cm h^{-1}) and naturally decanted, leads to the following conclusions:

1. The cellular-to-dendrite transition, observed through increasing solidification rates, is characterized by different substructure stages: (1) regular cells, (2) flanged cells or cellular dendrites, (3) cellular dendrites exhibiting the start of period lateral branching and (4) dendrites.

2. The free dendrites obtained by the decanting technique are quite similar to the dendrite

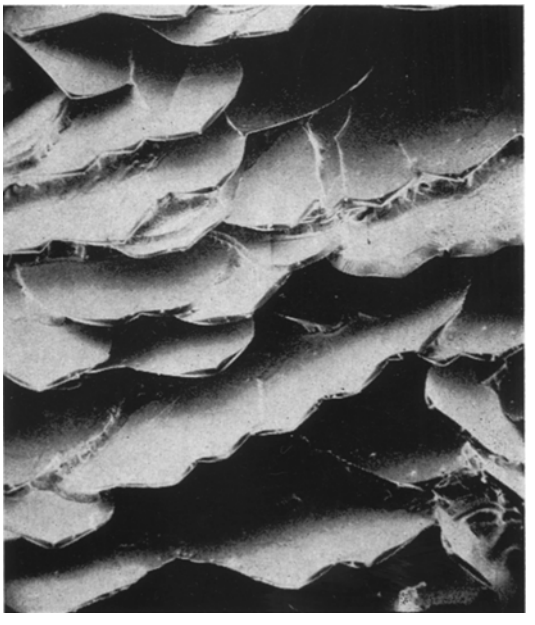

Figure 10 Scanning electron image of the lamella obtained by solidification of interdendritic liquid during decantation. ($\times$ 100).

substructure observed in unidirectionally solidified bars (stage 4).

3. The growth direction of the primary branches is parallel to ⟨100⟩ of the cubic lattice, the secondary branches are also parallel to these ⟨100⟩ directions. The cellular dendrites and dendrites are aligned in straight rows.

4. Microsegregation and Ta loss during solidification occurs with the formation of a white core in the interior of dendrites in some growth conditions.

Acknowledgements

The authors would like to thank Dr E. Ruedl and Mr D. Quataert for the help in crystallographic determination. Technical assistance was rendered by Miss Staroste, Messrs R. Baranzini, G. Bignoli, E. Haine, J. Lemaitre, L. Mammarella and A. Misirocchi. Thanks are also due to Professor J. C. Bilello of the Department of Materials Science, State University of New York for his helpful criticism and advice.

References

1. J. DEJACE, R. MATERA and G. PIATTI, *J. Mater. Sci* **8** (1973) 754.
2. G. BEGHI, D. BOERMAN, R. MATERA and G. PIATTI, "Verbundwerkstoffe" (Deutsche Gesellchaft für Metallkunde, Frankfurt, 1972) p. 102.
3. D. BOERMAN, J. DEJACE, R. MATERA and G. PIATTI, Annual Report (1971) of Ispra Joint Research Center Euratom. EUR 4842, p. 248.
4. G. A. CHADWICK, *Progr. Mat. Sci.* **12** (1963) 97.
5. F. R. MOLLARD and M. C. FLEMINGS, *Trans. Met. Soc. AIME* **239** (1967) 1534.
6. H. E. CLINE, *ibid* **242** (1968) 1613.
7. F. WEINBERG and B. CHALMERS, *Canad. J. Phys.* **29** (1951) 382.
8. A. ROSENBERG and W. A. TILLER, *Acta Met.* **5** (1957) 565.
9. G. A. CHADWICK, *ibid* **10** (1962) 1.
10. C. D. STATMAN and C. R. KOTLER, *J. Crystal Growth* **10** (1971) 115.
11. H. D. BRODY and M. C. FLEMINGS, *Trans. Met. Soc. AIME* **236** (1966) 615.
12. K. N. STREET, F. C. ST-JOHN and G. PIATTI, *J. Inst. Met.* **9** (1967) 526.
13. L. R. MORRIS and W. C. WINEGARD, *J. Crystal Growth* **6** (1969) 61.
14. T. Z. KATTAMIS and M. C. FLEMINGS, *Trans. Met. Soc. AIME* **233** (1965) 992.
15. F. WEINBERG and R. K. BUHR, Iron Steel Inst. London (1968) Publ. no 110, p. 295.
16. H. TRESH, M. BERGERON, F. WEINBERG and R. K. BUHR, *Trans. Met. Soc. AIME* **242** (1968) 853.
17. R. J. SCHWENSFEIR JUN. and CHU TZU WU, *Mater. Sci. Eng.* **8** (1971) 284.
18. M. J. STEWART and F. WEINBERG, *Met. Trans.* **3** (1972) 333.
19. F. WEINBERG and E. TEGHTSOONIAN, *ibid* **3** (1972) 93.
20. G. R. KOTLER, K. W. CASEY and G. S. COLE, *ibid* **3** (1972) 723.
21. H. NOVOTNY and H. OESTERREICHER, *Monatsh. Chem.* **95** (1964) 982.
22. W. A. TILLER and J. W. RUTTER, *Canad. J. Phys.* **34** (1956) 96.
23. M. A. AUDERO and H. BILONI, *J. Crystal Growth* **12** (1972) 297.
24. W. KURZ and B. LUX, *Z. Metallkunde* **63** (1972) 509.
25. B. CHALMERS, "Principles of solidification", (John Wiley, New York, 1964).
26. T. S. PLASKETT and W. C. WINEGARD, *Canad. J. Phys.* **38** (1960) 1077.
27. E. L. HOLMES, J. W. RUTTER and W. C. WINEGARD, *ibid* **35** (1957) 1223.
28. J. O. COULTHARD and R. ELLIOTT, "The solidification of Metals" (Iron and Steel Inst., London, 1968) Publ. no 110, p. 61.
29. G. J. DAVIES, *ibid* p. 66.
30. A. B. MICHAEL and M. B. BEVER, *J. Metals*, January (1954) 47.
31. N. KARLSSON, *J. Inst. Met.* **79** (1951) 391.
32. A. SHUNK, "Constitution of Binary Alloy" (McGraw-Hill, New York, 1969).

Received 1 October 1973 and accepted 13 June 1974.